Absorption and Emission Study of 2′,7′-Difluorofluorescein and Its Excited-State Buffer-Mediated Proton Exchange Reactions

Angel Orte,[†] Luis Crovetto,[†] Eva M. Talavera,[†] Noël Boens,[‡] and Jose M. Alvarez-Pez*,[†]

Department of Physical Chemistry, University of Granada, Cartuja Campus, Granada 18071, Spain, and Department of Chemistry, Katholieke Universiteit Leuven, Celestijnenlaan 200 F, 3001 Heverlee (Leuven), Belgium

Received: July 20, 2004; In Final Form: October 15, 2004

2′,7′-Difluorofluorescein (Oregon Green 488) is a new fluorescein-based dye, which has found many applications, above all in biochemistry and neurosciences, and its use has become very popular in the last years. In recent years, we have been investigating the excited-state proton exchange reactions of fluorescein and the effect of suitable proton acceptors and donors which promote these reactions. The excited-state proton transfer reactions may appreciably influence the fluorescence results when using these dyes. We present steady-state emission evidence that acetate buffer species promote an excited-state proton transfer between neutral, monoanionic, and dianionic forms of 2′,7′-difluorofluorescein. The time course of the excited species in this reaction was characterized through time-resolved fluorescence measurements, and the kinetics of the reaction was solved by using the global compartmental analysis. A previous identifiability study on the compartmental system set the conditions to design the fluorescence decay surface. This is the first experimental system, studied within this kinetic model, solved under identifiability conditions through global compartmental analysis. The recovered rate constant values for deactivation were 2.94×10^8 s^{-1} for the monoanion and 2.47×10^8 s^{-1} for the dianion, whereas the rate constant values of the buffer-mediated excited-state reaction were 9.70×10^8 and 1.79×10^8 M^{-1} s^{-1} for the deprotonation and protonation, respectively. With these values, a $pK_a^* = 4.02$ was obtained. In this work, we additionally provide an absorption study, including acid−base equilibria, determination of ground-state pK_a values (1.02, 3.61, and 4.69), and recovery of molar absorption coefficients of every prototropic species, including absorption and NMR evidence for the existence of three tautomers in neutral species. Steady-state emission spectra of 2′,7′-difluorofluorescein in aqueous solution are also described, where the strong photoacid behavior of the cation is noteworthy.

Introduction

Fluorescein is a well-known dye widely used in multiple biological and biochemical applications. However, it undergoes photobleaching reactions upon intense illumination. In addition, its absorption and fluorescence characteristics show important pH-dependence at near-neutral pH (∼6.8−7.4).[1] New fluorophores are now commercially available which reduce these fluorescein drawbacks. One of the most popular of these new dyes is 2′,7′-difluorofluorescein (Oregon Green 488, OG488). OG488 shows more resistance to photodegradation than fluorescein,[1,2] and it has unchanging absorption and fluorescence properties in the physiological pH range.[1] OG488 has been used in multiple applications as a fluorescent protein label, OG488-based fluorescent Ca^{2+} indicators,[1,3] in fluorescence imaging,[1,4] anisotropy probe,[5] and so forth. Nevertheless, there is a lack of basic spectroscopic information about OG488 in the literature. For instance, only values for a pK_a (4.8)[2] and dianion absorption coefficient at the maximum of the visible band (82 400−87 000 M^{-1} cm^{-1})[1,2] are found. This encouraged us to provide basic absorption and fluorescence data and describe ground-state acid−base equilibria in the first part of this work.

We have been investigating the effect of proton acceptors and donors in the excited-state proton transfer (ESPT) reactions of fluorescein for several years. We have demonstrated that the presence of an appropriate proton acceptor or donor, such as a buffer species, promotes an ESPT reaction between monoanion and dianion species of fluorescein. We characterized these excited-state processes in 1 M phosphate buffer aqueous solutions through steady-state[6] and time-resolved[7] fluorimetry. Since fluorescein is commonly used in several biological applications in which a proton acceptor or donor may be present, it is of interest to consider possible excited-state reactions that might cause a misevaluation of experimental fluorescence data. An important aspect concerning this is to establish whether amino acids with acidic (or basic) side chains are able to induce fluorescein excited-state proton-transfer reactions when labeling proteins. We studied the system fluorescein−(±)-*N*-acetyl aspartic acid (*N*-AcAsp) as a model system which mimics the interaction of the aspartic acid residues with fluorescein as a fluorescent label in native proteins. In that study, we found that *N*-AcAsp also acts as a suitable proton acceptor or donor, promoting an excited-state proton transfer. The kinetics of this excited-state process was characterized from time-resolved fluorescence measurements, and the analysis was done within the framework of a new global compartmental analysis method.[8]

According to our previous data, OG488 also shows proton exchange reactions during its excited-state decay time.[9] Some of these reactions are spontaneous, and others need a suitable proton acceptor or donor present at sufficiently high concentration. In these reactions, the less fluorescent monoanion is

* To whom correspondence should be addressed. E-mail address: jalvarez@ugr.es.
[†] University of Granada.
[‡] Katholieke Universiteit Leuven.

10.1021/jp046786v CCC: $30.25
Published on Web 01/19/2005

transformed to the dianion (with higher quantum yield), and vice versa, during the decay times of the excited species. Since proteins and biomolecules in general have chemical groups that can act as proton acceptors or donors and the buffer in which they are dissolved can also behave as an appropriate proton acceptor or donor, the excited-state reactions might influence the steady-state fluorescence signals when the dye is used for labeling biomolecules. For this reason, we have initiated a program to determine the reaction models as well as the kinetic and spectral parameters for these excited-state proton exchange reactions, allowing a more correct interpretation of the fluorescence experimental data when OG488 is used as fluorescent label.

Fluorescence decay curves of excited-state systems are often well described as a multiexponential function, in terms of decay times and corresponding pre-exponential factors. However, the underlying significant parameters, which describe the dynamic behavior of the system, are the rate constants defining the excited-state kinetics and the spectral parameters related to excitation and emission. A multidimensional fluorescence decay data surface, measured under various experimental conditions, is required to determine those fundamental parameters. Single curve and classical simultaneous (global) analyses of multiple decays provide values of relaxation times and pre-exponentials. Global analysis leads to a more accurate parameter recovery, since relationships between individual decays are taken into account. Thus, some parameters can be linked between related experiments (e.g., the decay times do not vary over decay traces collected at various emission wavelengths for the same sample).[10−12] These recovered decay times and pre-exponential factors can be used to test several kinetic models and calculate the rate constants and the species-associated spectra. Hence, the recovery of these parameters requires a two-step analysis process.

Global compartmental analysis has recently been introduced into photophysics.[13,14] However, compartmental models are being widely used in many fields such as pharmacokinetics, ecology, engineering, and so forth.[15] An appropriate description of the excited-state processes can be carried out within the framework of compartmental analysis, since a compartment is a subsystem of a species acting in an unique kinetic way. The main advantage of global compartmental analysis lies in the possibility of recovering directly, with high accuracy and precision, the underlying parameters of the kinetic model (i.e., rate constants and spectral parameters associated with excitation and emission).[16] The determination of the parameters of interest is done by a single-step analysis of the complete decay data surface.

In this paper we shall analyze the fluorescence decay surface of OG488 undergoing intermolecular two-state excited-state processes with added acetate buffer in terms of compartments. The relevant parameters (rate constants and spectral parameters) were recovered uniquely. The different experimental conditions, defining the fluorescence decay surface, were chosen according to the identifiability study for this compartmental model published elsewhere.[17] This is the first experimental system of an excited-state proton-transfer reaction promoted by species of a suitable proton acceptor or donor analyzed using global compartmental analysis under identifiability conditions.

Theory

Scheme 1 represents the dynamic, linear, time-invariant, intermolecular system studied. It consists of two distinct types of ground-state species and their corresponding excited-state species. Both species are two different prototropic forms of the considered dye. Thus, the ground-state species are related through the acid−base equilibria, determined by the corresponding pK_a. Excited-state species **1*** and **2*** are created upon photoexcitation, and they can decay by fluorescence (F) and nonradiative (NR) processes. We include those decay processes in rate constant k_{0i} (equal to $k_{Fi} + k_{NRi}$) for species *i**. In this study, we consider the excited-state process promoted by species of an added buffer, HR and R. Hence, HR could promote an excited-state protonation with **2***, represented by rate constant k^b_{12}. Likewise, R could react with **1*** resulting in an excited-state deprotonation, whose rate constant is denoted by k^b_{21}. We also include the deprotonation of excited state **1*** (represented by rate constant k_{21}), and excited-state reaction of **2*** with aqueous protons, with rate constant denoted by k_{12}.

SCHEME 1: Kinetic Model of an Excited-State Proton Transfer Reaction, Promoted by a Suitable Proton Acceptor or Donor[a]

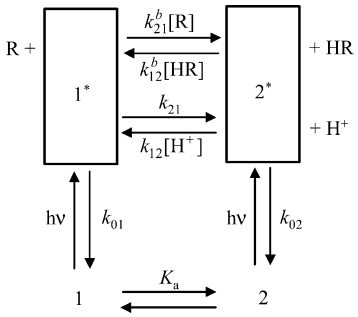

[a] **1** and **2** are the ground-state conjugate acid−base forms of the fluorophore, whereas **1*** and **2*** are the corresponding excited species. R and HR are the acid−base species of the proton acceptor or donor.

When exciting the system with a δ-pulse at time $t = 0$, which does not significantly alter the ground-state concentrations, the time course of the concentrations of the excited-state species **1*** and **2*** is described by the first-order differential equation

$$\dot{\mathbf{x}}(t) = \mathbf{A}\mathbf{x}(t) \tag{1}$$

$\mathbf{x}(t)$ is the 2×1 vector function of the concentrations of the excited-state species **1*** and **2***:

$$\begin{pmatrix} x_1(t) \\ x_2(t) \end{pmatrix} = \begin{pmatrix} [\mathbf{1}^*](t) \\ [\mathbf{2}^*](t) \end{pmatrix} \tag{2}$$

$\dot{\mathbf{x}}(t)$ denotes its time derivative, and $\mathbf{A}$ is the 2×2 compartmental matrix:

$$\mathbf{A} = \begin{bmatrix} -(k_{01} + k_{21} + k^b_{21}[\mathrm{R}]) & k_{12}[\mathrm{H}^+] + k^b_{12}[\mathrm{HR}] \\ k_{21} + k^b_{21}[\mathrm{R}] & -(k_{02} + k_{12}[\mathrm{H}^+] + k^b_{12}[\mathrm{HR}]) \end{bmatrix} \tag{3}$$

The fluorescence impulse response function, $f(\lambda^{em},\lambda^{ex},t)$, at emission wavelength λ^{em} and excitation at λ^{ex}, is given by eq 4[14] and depends on λ^{ex}, λ^{em}, $[H^+]$, and the total buffer concentration ($C^{buff} = [R] + [HR]$).

$$f(\lambda^{em},\lambda^{ex},t) = \kappa \tilde{\mathbf{c}} \mathbf{U} \exp(t\Gamma) \mathbf{U}^{-1} \tilde{\mathbf{b}} \tag{4}$$

In this equation, we assume that the 2×2 compartmental matrix $\mathbf{A}$ has two linearly independent eigenvectors $\mathbf{U}_1$ and $\mathbf{U}_2$ associated with the eigenvalues γ_1 and γ_2, respectively, that is, $\mathbf{A} = \mathbf{U}\Gamma\mathbf{U}^{-1}$ with $\mathbf{U} = [\mathbf{U}_1, \mathbf{U}_2]$ and with $\mathbf{U}^{-1}$ being the inverse of the matrix of the eigenvectors, Γ is the diagonal matrix of two eigenvalues, and $\exp(\Gamma t) = \mathrm{diag}[\exp(\gamma_1 t), \exp(\gamma_2 t)]$. $\mathbf{U}$ and

$\exp(\Gamma t)$ are functions of the rate constants k_{ij} and the concentrations [R], [HR], and [H^+].

The concentrations of species i^* at time zero are defined by $\mathbf{x}(0) = \mathbf{b}$ where $\mathbf{b}$ is the 2×1 vector with elements b_i ($i = 1, 2$). $\mathbf{b}$ depends on the excitation wavelength λ^{ex} and [H^+]. $\tilde{\mathbf{b}}$ is the 2×1 vector with normalized elements of $\mathbf{b}$. The elements $\tilde{b}_i$ are calculated by[14]

$$\tilde{b}_i = \frac{\epsilon_i \alpha_i}{\sum_i \epsilon_i \alpha_i} \tag{5}$$

where ϵ_i is the molar absorption coefficient of the ith compartment and α_i is the molar fraction of each form in the ground-state.

$\tilde{\mathbf{c}}$ is the 1×2 vector of the normalized emission weighting factors ($\tilde{c}_i = c_i/\sum_i c_i$) of species i^* at emission wavelength λ^{em},[14]

$$c_i(\lambda^{em}) = k_{Fi} \int_{\Delta\lambda^{em}} \rho_i(\lambda^{em})\, d\lambda^{em} \tag{6}$$

where k_{Fi} is the fluorescence rate constant of i^*, $\Delta\lambda^{em}$ is the emission wavelength interval around λ^{em} where the fluorescence signal is monitored, and $\rho_i(\lambda^{em})$ is the emission density of i^* at λ^{em} defined by[14]

$$\rho_i(\lambda^{em}) = F_i(\lambda^{em},\lambda^{ex}) / \int_{\text{full emission band}} F_i(\lambda^{em},\lambda^{ex})\, d\lambda^{em} \tag{7}$$

where the integration extends over the whole steady-state fluorescence spectrum F_i of species i^*.

Finally, κ is a proportionality constant given by

$$\kappa = \sum_{\forall_i} b_i \sum_{\forall_i} c_i \tag{8}$$

The use of κ, $\tilde{b}_i$, and $\tilde{c}_i$ allows one to link $\tilde{b}_i$ and $\tilde{c}_i$ in the data analysis so that the collected decay traces are not required to be scaled. Indeed, $\tilde{\mathbf{b}}$ depends on λ^{ex} and [H^+] (or pH), whereas $\tilde{\mathbf{c}}(\lambda^{em})$ depends on the emission wavelength only. In our implementation of global compartmental analysis, one fits directly for the rate constants k_{01}, k_{21}, k_{02}, k_{12}, k_{12}^b, k_{21}^b the normalized zero-time concentrations $\tilde{b}_1$ of species **1*** and the normalized spectral emission weighting factors $\tilde{c}_1(\lambda^{em})$ of species **1***.

Equation 4 can be written in the common biexponential format (with $t \geq 0$):

$$f(t) = p_1 e^{\gamma_1 t} + p_2 e^{\gamma_2 t} \tag{9}$$

The eigenvalues γ_i ($i = 1, 2$) of the compartmental matrix $\mathbf{A}$ are related to the decay times τ_i ($i = 1, 2$) according to

$$\gamma_i = -1/\tau_i \tag{10}$$

and are given by

$$\gamma_i = \frac{a_{11} + a_{22} \pm \sqrt{(a_{22} - a_{11})^2 + 4a_{12}a_{21}}}{2} \tag{11}$$

with a_{ij}, the ijth element of the compartmental matrix $\mathbf{A}$ (eq 3).

The pre-exponentials, p_i, of eq 9 are related to compartmental parameters through the following equations:

$$p_1 = \kappa(\tilde{c}_1\beta_{11} + \tilde{c}_2\beta_{21}) \tag{12a}$$

$$p_2 = \kappa(\tilde{c}_1\beta_{12} + \tilde{c}_2\beta_{22}) \tag{12b}$$

$$\beta_{11} = \frac{[\tilde{b}_1(\gamma_2 - a_{11}) - \tilde{b}_2 a_{12}]}{(\gamma_2 - \gamma_1)} \tag{13a}$$

$$\beta_{12} = -\frac{[\tilde{b}_1(\gamma_1 - a_{11}) - \tilde{b}_2 a_{12}]}{(\gamma_2 - \gamma_1)} \tag{13b}$$

$$\beta_{21} = \frac{[\tilde{b}_2(\gamma_2 - a_{22}) - \tilde{b}_1 a_{21}]}{(\gamma_2 - \gamma_1)} \tag{13c}$$

$$\beta_{22} = -\frac{[\tilde{b}_2(\gamma_1 - a_{22}) - \tilde{b}_1 a_{21}]}{(\gamma_2 - \gamma_1)} \tag{13d}$$

Materials and Methods

Reagents and Solutions. 2′,7′-Difluorofluorescein (Oregon Green 488) was purchased from Molecular Probes (Eugene, OR). Acetic acid (HOAc), sodium acetate (NaOAc), sodium hydroxide, sodium perchlorate, and perchloric acid (analysis grade) were from Merck. All products were used without further purification. Stock solutions of 2′,7′-difluorofluorescein (10^{-4} M) in 1.27×10^{-3} M NaOH, HOAc (2 M), and NaOAc (2 M) were prepared using MilliQ water. The required volumes of OG488, sodium acetate, acetic acid, perchloric acid, sodium perchlorate, and sodium hydroxide stock solutions were used to obtain the desired concentrations of OG488, pH, and buffer concentration. OG488 solutions were kept cool in the dark when not in use to avoid possible deterioration by exposure to light and heat as occurs with fluorescein.[18] Deuterated dimethyl sulfoxide (DMSO) and methanol were used as solvents in ^{1}H NMR spectra.

Absorption and Steady-State Fluorescence Measurements. An L configuration Perkin-Elmer LS 55 spectrofluorometer with a temperature-controlled cell holder was used to acquire steady-state fluorescence spectra. Absorption spectra were recorded on a GBC Cintra 10e UV−vis spectrophotometer with a temperature-controlled cell holder. All measurements were made at room temperature. Cuvettes (10 mm × 10 mm) were used for both absorption and steady-state fluorescence measurements.

NMR Spectrometer. ^{1}H NMR spectra were recorded on a BRUKER AM300 spectrometer, at 300 MHz. It has a temperature-controlled 5-mm QNP probe for ^{1}H, ^{13}C, ^{19}F, and ^{31}P and accessories for solid CP/MAS NMR spectra.

Nonlinear Least-Squares Fitting. The fitting processes of absorption and steady-state fluorescence intensity data were performed using Origin 6.0 routines based on Marquardt's algorithm. The goodness-of-fitting criteria were the regression coefficient (r^2) and the visual similarity between the fitted function and the experimental data. The dependency of the recovered parameters was also checked via the dependency coefficient which indicates whether the equation is overparametrized. A dependency value below 0.96 is acceptable.[19]

Time-Resolved Fluorescence Measurements. Fluorescence decay traces were recorded on a laser-based system with single-photon timing detection. This system employs a regeneratively mode-locked Ti−sapphire laser, pumped by an argon ion laser. The system provides tuning of excitation wavelengths over a range from 240 to 1300 nm and stable 1−2 ps pulse trains. The devices used to achieve this setup are a pulse selector, a flexible harmonic generator based on frequency doubling and sum frequency mixing, and a synchronously pumped optical parametric oscillator. A Glan−Thomson polarizer allows linear

SCHEME 2: Kinetic Model of the Excited-State Proton Transfer Reaction between Monoanion (M) and Dianion (D) of OG488, Promoted by Acetic Acid/Acetate as Proton Acceptor/Donor

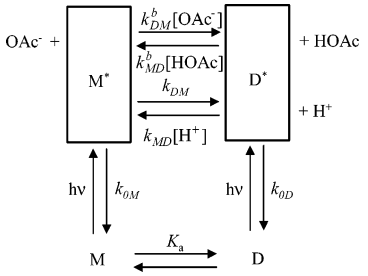

polarization of the excitation pulses and was set at magic angle (54.7°) polarization of the emission beam with respect to the excitation polarization. A cooled microchannel plate photomultiplier was used after a double subtractive monochromator to detect the emission. Full details of the instrument have been reported elsewhere.[20]

Fluorescence decay traces were collected using 10 mm × 10 mm cuvettes along 4096 channels. The time increments per channel were 5.94 and 2.46 ps. Histograms of the instrument response function (using commercial Ludox scatterer) and sample decays were recorded until the typical value of 10^4 counts in the peak channel was reached.

The excitation wavelength was 420 nm, which excites preferentially the monoanion instead of the dianionic form. Emission wavelengths were 490, 515, 525, 550, 570, 580, and 600 nm. Decay traces of solutions of OG488 without added buffer and in the presence of 1 M acetate buffer were recorded.

Program Implementation. The global compartmental analysis of the collected fluorescence decay surfaces was implemented in a general global analysis program using Gaussian-weighted nonlinear least-squares fitting based on Marquardt−Levenberg minimization.

The compartmental model considered (Scheme 2) includes two-state excited-state proton transfer, promoted by acetate buffer species, between monoanion and dianion of OG488. The global fitting parameters were k_{0M}, k_{0D}, k_{MD}, k_{DM}, k^b_{MD}, k^b_{DM}, $b_M(\mathrm{pH})$, and $\tilde{c}_M(\lambda^{em})$ and the local scaling factors κ. Scheme 3 shows the linking scheme of adjustable parameters over the complete decay surface. We note that decay traces in the absence of buffer do not provide any information about k^b_{MD} or k^b_{DM}. Hence, they are not linked over decays in the absence of buffer. The additional decays in the absence of buffer, however, are needed to perform a global compartmental analysis under identifiability conditions.[17]

Results

Absorption Measurements and Ground-State Equilibria of OG488. Becuase of lack of descriptive information about ground-state acid−base equilibria of OG488 in aqueous solution, we decided to carry out a study to determine its equilibrium constants and visible spectral characteristics. The visible absorption spectra of aqueous solutions of OG488 as a function of pH in the range 0−12 were recorded. With pH variation, abrupt changes in absorbance were clearly observed. The experimental absorption spectra of solutions at different pH values show pH-induced transitions due to ground-state proton reactions, and these occur in regions of pH dictated by the ground-state pK_a values. The amplitude of the transitions and the general appearance of the absorption versus pH graphs depend on the wavelength used in the absorption measurements. Three transitions and two different isosbestic points could be distinguished. Since fluorination at positions 2′ and 7′ does not alter the acid−base groups available in fluorescein, we assume that OG488 in aqueous solution presents four visible absorbing prototropic forms, namely, cation (C), neutral (N), monoanion (M), and dianion (D). Thus, three ground-state pK_a's are involved. Furthermore, three different tautomeric modifications are described for neutral fluorescein: a quinoid form, a zwitterion, and a lactonic tautomer. We assume that these three modifications could also be found in the bifluorinated derivative OG488. According to this, the acid−base and tautomeric equilibria taken into account in this work are shown in Figure 1.

Assuming that the system follows Beer's law, at any wavelength and pH, the absorbance A is given by the expression

$$A = C^{\mathrm{OG488}}\left(\sum_i \alpha_i \epsilon_i\right) d \tag{14}$$

where C^{OG488} is the total concentration of OG488, α_i is the fraction of OG488 in the ith prototropic form, ϵ_i is the molar absorption coefficient of the ith prototropic form of OG488, and d is the optical path length. The values of ϵ_i depend on wavelength, whereas the values of α_i depend on pH and ground-state acidity constants (pK_a values). From simple equilibrium theory, we can write the following expressions for the relationships between α_i, the ground-state acidity constants for cation/neutral (K_C), neutral/monoanion (K_N), and monoanion/dianion (K_M), and $[H^+]$:[6]

$$\alpha_C = \frac{[H^+]^3}{P} \tag{15}$$

$$\alpha_N = \frac{K_C[H^+]^2}{P} \tag{16}$$

$$\alpha_M = \frac{K_C K_N [H^+]}{P} \tag{17}$$

$$\alpha_D = \frac{K_C K_N K_M}{P} \tag{18}$$

$$P = [H^+]^3 + K_C[H^+]^2 + K_C K_N [H^+] + K_C K_N K_M \tag{19}$$

Dianion absorption coefficients at wavelengths between 350 and 550 nm were estimated through linear regression of absorbance versus concentration data from spectra collected at 0.08 M sodium hydroxide concentration, assuming that no species other than dianion exists at this pH. Beer's law linearity was achieved from 1.0×10^{-6} up to 2×10^{-5} M in OG488. Figure 2 shows the recovered absorption coefficients. The dianion absorption spectrum is formed by a simple band centered at 490.5 nm and a shoulder around 450 nm. The spectrum maximum at 490.5 nm shows an absorption coefficient of 86 400 ± 700 M^{-1} cm^{-1}. This result is in good agreement with those found in the literature: 82 400[2] and 87 000[1] M^{-1} cm^{-1} at 490 nm. We emphasize the spectral similarity with fluorescein whose dianion form shows the same spectral shape and absorption coefficient at the maximum between (depending on literature) 76 900[21] and 87 700[22] M^{-1} cm^{-1}.

Next, we analyzed the experimental absorbance versus pH, at three different OG488 concentrations (5×10^{-6}, 7.5×10^{-6}, and 10^{-5} M) in the pH range between −0.12 and 12.40. We implemented an iterative global nonlinear least-squares curve

SCHEME 3: Linking Scheme for the Global Compartmental Analysis[a]

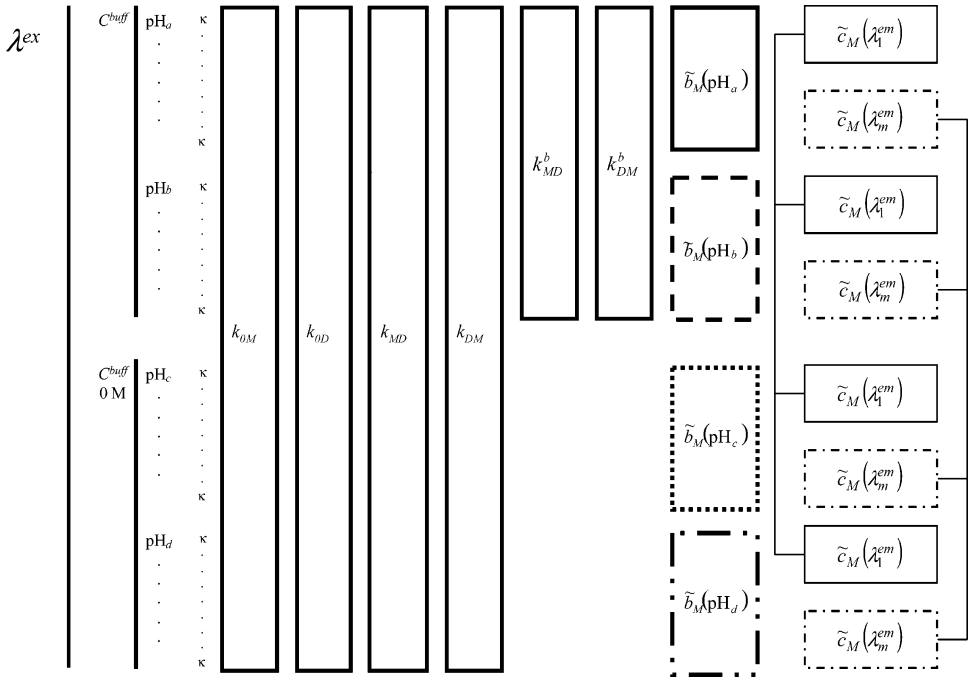

[a] Decays due to a single excitation wavelength (λ^{ex}) were recorded at m different emission wavelengths (λ^{em}) and in the absence ($C^{buff} = 0$) and the presence (C^{buff}) of buffer. Boxed and/or connected parameters in the same line type indicate linked parameters, whereas κ denotes the local scaling factors. The rate constants k_{ij} are linked over the entire surface, whereas k^b_{ij} are only linked over decays in the presence of proton acceptor or donor. Excitation parameters $\tilde{b}_M$ are linked at the same pH value, and emission parameters $\tilde{c}_M$ are linked at the same emission wavelength.

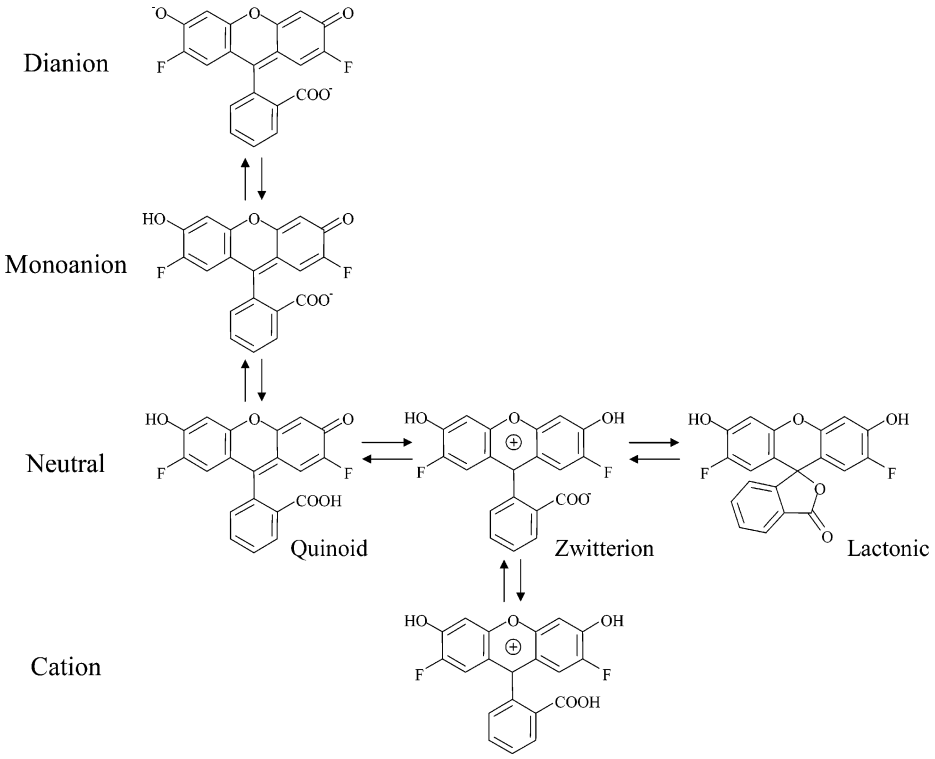

Figure 1. Different prototropic forms and acid−base equilibria of OG488 in aqueous solution.

fitting method, according to the following equation (based on eqs 14−19):

$$\frac{A(\lambda)}{C^{OG488}} = \alpha_C\epsilon_C(\lambda) + \alpha_N\epsilon_N(\lambda) + \alpha_M\epsilon_M(\lambda) + \alpha_D\epsilon_D(\lambda) \quad (20)$$

The global fitting of the complete wavelength range was performed using ϵ_D as known fixed parameter, ϵ_C, ϵ_N, and ϵ_M as locally adjustable parameters at each wavelength, and pK_C, pK_N, and pK_M as globally linked adjustable parameters. Beer's law for four prototropic species became the best model to fit the experimental absorption data. A three-species model was insufficient to fit the data correctly, while five species resulted in higher parameter dependency and did not improve the statistical goodness-of-fit parameters. Plots of the experimental A/C^{OG488} versus pH curves were well fitted by the nonlinear

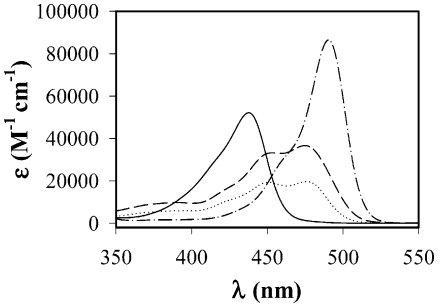

Figure 2. Plot of the molar absorption coefficients vs wavelength for the cationic (—), neutral (···), monoanionic (- - -), and dianionic (- · -) species of OG488.

TABLE 1: pK_a Values Recovered from Global Nonlinear Least-Squares Fitting of the Surface A/C^{OG488} vs pH

	value	dependency	literature
pK_C	1.016 ± 0.007	3×10^{-5}	
pK_N	3.610 ± 0.010	0.156	
pK_M	4.688 ± 0.004	0.156	4.8[a]

[a] Sun et al.[2]

least-squares method. In the curve fitting process, the estimated parameter values were independent of the initial guesses assigned to these parameters. Figure 2 also shows the recovered absorption spectral profiles of cationic, neutral, and monoanionic species of OG488. The cation presented a simple band centered at 437.5 nm with an absorption coefficient of 55 700 ± 200 M^{-1} cm^{-1}, while neutral and monoanionic species showed very similar spectra with two maxima at 451.5 and 476 nm. Neutral absorption coefficients at these maxima were 19 200 ± 200 and 19 500 ± 600 M^{-1} cm^{-1}, respectively. Absorption coefficients of the monoanionic form at these wavelengths were 32 300 ± 400 and 35 600 ± 900 M^{-1} cm^{-1}, respectively. Table 1 shows the recovered pK_a values. The dependency coefficients of the recovered parameters are also shown. They indicate that the equation is in fact not overparametrized. The decrease in each pK_a value upon fluorination with respect to fluorescein (pK_C = 2.1−2.25, pK_N = 4.23−5.1, pK_M = 6.31−6.44, depending on literature)[21−23] should be noted. Fluorination provides a higher polarity to the aromatic xanthene group, which produces higher acidity in acid−base groups. The same behavior is found in other fluorescein derivatives with electron withdrawing substituents, such as 2′,7′-dichlorofluorescein (pK_C = 0.47, pK_N = 3.50, and pK_M = 4.95).[24]

As previously cited, in fluorescein, three tautomeric forms are described for neutral species: quinoid (monoanion-like structure), zwitterionic (cation-like structure), and lactonic.[23] It can be seen in Figure 2 that the neutral OG488 molecule has a similar shape and lower absorbance as the monoanion form. This finding indicates that the neutral quinoid form, which has the same chromophore group as monoanion, is the preferentially absorbing tautomer. On the contrary, the lactonic modification does not alter visible absorption, since the carboxyl and xanthene groups are not conjugated to each other. We decomposed the neutral spectrum into cation and monoanion contributions to provide the contribution of zwitterionic and quinoid forms to the neutral spectrum. Since the cation does not absorb in the 480−500 nm wavelength range, we scaled the monoanion spectrum to the neutral in this wavelength range, obtaining a factor of 0.576. Then, this contribution was subtracted from the complete spectrum of the neutral, resulting in a cation-like spectrum. This contribution corresponded to the cation spectrum multiplied by 0.034. These factors are directly related to the percentage of the total molecules in each form, monoanion-like and cation-like. Therefore, the decomposition of the neutral form absorption spectrum yielded a contribution of 57.6% of quinoid tautomer and 3.4% of zwitterionic. The rest (39.0%) was assigned to the lactonic modification, which does not absorb in the visible range because of the broken conjugation of the xanthene moiety. The spectral decomposition of the neutral spectrum is shown in Figure 3. In contrast to OG488, in fluorescein, the main modification is the lactone form (62.5%),[23] and the zwitterion is present at percentages between 22 and 25%.[23,25] The differences found between OG488 and fluorescein can be explained according to the mesomeric +M effect of fluorine atoms in the ring, as can be seen in Figure 4. This effect produces a partial negative charge in the xanthene moiety, which destabilizes the zwitterionic and lactonic modifications. This is consistent with the σ_R value for fluorine substituents (−0.32),[26] applicable in the absence of direct conjugation between substituent and reaction center, the type of system that would fit the Hammet equation.[26]

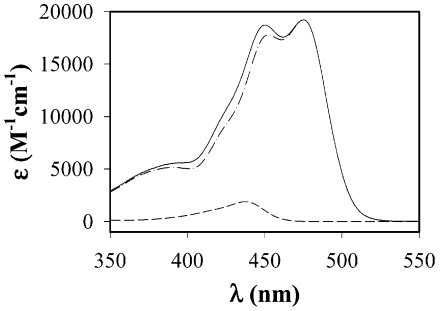

Figure 3. Spectral decomposition of the neutral absorption spectrum (—) in the contributions of the monoanion (factor of 0.576, - · -) and the cation (factor of 0.034, - - -) absorption spectra.

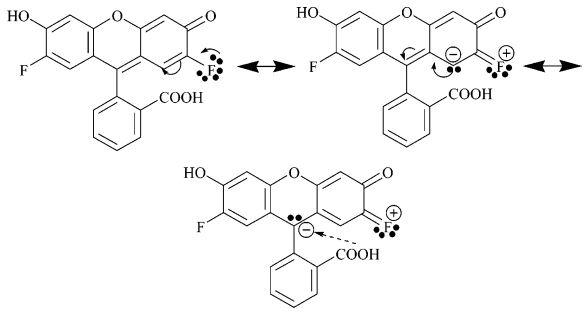

Figure 4. Mesomeric +M effect of the fluorine atoms in 2′,7′-difluorofluorescein.

To obtain more evidence for the presence of the three neutral tautomers, we recorded the proton NMR spectra of OG488 in deuterated DMSO and methanol. Table 2 shows the chemical shifts (δ), multiplicity, coupling constants, and intensity of each signal. The results were in excellent agreement with those reported by Sun et al.[2] for OG488 in deuterated DMSO. Coupling constants $^1H-^1H$ (around 7.5 Hz) and $^1H-^{19}F$ (11.1 Hz) and multiplicity helped us to assign all the signals to the corresponding hydrogen atoms. The main feature was the presence of a single signal at low fields in DMSO. This signal was due to −OH groups in xanthene ring. The signal was not present in methanol because of proton exchange with solvent molecules. The absence of a signal corresponding to a −COOH group could indicate that the quinoid tautomer did not make an important contribution in this solvent. Nevertheless, a fast proton exchange is possible, which would make the −COOH signal undetectable. The intensity of the signal at 10.73 ppm did not exactly correspond to two hydrogen atoms, which would indicate the unique presence of lactonic and zwitterionic species. The

TABLE 2: Signals of ^{1}H NMR[a] Spectra of OG488 in Deuterated DMSO and Methanol

chemical shift (δ)[b]	multiplicity	coupling constants (Hz)	intensity	number of H
		DMSO Solvent		
10.73	singlet		5.85	≈2
7.98	doublet	7.4	3.22	1
7.79	triplet	7.0	6.68	1
7.72	triplet	7.3		1
7.28	doublet	7.5	3.44	1
6.86	doublet	7.5	6.25	2
6.46	doublet	11.3	6.12	2
		Methanol Solvent		
8.07	doublet	7.6	0.709	1
7.82	triplet	7.4	1.262	≈2
7.75	triplet	7.2		
7.27	doublet	7.3	0.752	1
6.84	doublet	7.5	1.009	≈2
6.43	doublet	11.1	1.089	≈2

[a] Electromagnetic field frequency: 300 MHz. [b] Expressed in ppm of the main frequency.

lower intensity of this signal might be produced by a low contribution of quinoid form in equilibrium. Thus, evidence of the three forms was supported by ^{1}H NMR spectra. Therefore, the visible absorption and ^{1}H NMR spectra were in good agreement with the equilibria and structures shown in Figure 1.

Steady-State Fluorescence Features of Aqueous Solutions of OG488. We recorded the steady-state fluorescence emission spectra, at two excitation wavelengths (424 and 460 nm), of aqueous solutions of OG488 over a wide [H^+] range between 9.5 M $HClO_4$ and pH values up to about 12, by using perchloric acid and sodium hydroxide. Two different spectral profiles were detected in the pH range 12−3.44 (Figure 5a). At very high pH (11.65), only the dianion is present, and hence only this form emits. The dianion of OG488 has a fluorescence quantum yield near unity.[1,2] It showed an emission band centered on 515 nm, the mirror image of the dianion absorption spectrum. The second spectral profile was centered on 513 nm, but it showed a shoulder around 550 nm. We assumed that this spectral profile corresponded to the monoanion. At pH values between 0 and 5, the ground-state neutral form is also present. Since quinoid neutral tautomer is the main form in aqueous solution, the neutral steady-state fluorescence spectral profile should be identical to monoanion shape. In Figure 5b, the normalized spectra show that the spectral shape varies only slightly at pH below 3.44 down to 2 M $HClO_4$.

We note that cation emission was not detected at acid concentration below 2 M, although cation absorption is clearly observed in the [H^+] range between pH 2.12 and 2 M $HClO_4$. In the steady-state fluorescence spectrum of OG488 solution at 2 M perchloric acid concentration, a very low emissive contribution around 460 nm is detected, which can be better seen in the normalized spectrum of Figure 5b. Higher acid concentrations were used to observe the cation emission. In Figure 5c, emission spectra of solutions at $HClO_4$ concentrations between 9.5 and 3 M are shown. A simple emission band was detected at 9.5 M perchloric acid concentration, which rapidly changed to monoanion/neutral emission with decreasing acid concentration. While emission spectral shapes were changeable, absorption spectra were invariable at the cation absorption in this pH range. These features clearly indicate the excited-state deprotonation of cation form, since it turned to a super-photoacid upon excitation, as occurs in fluorescein,[27] naphthol, and other phenols.[28] The photoacid behavior of the cationic form and the kinetics of the excited-state proton-transfer reactions in this [H^+] range will be published elsewhere.

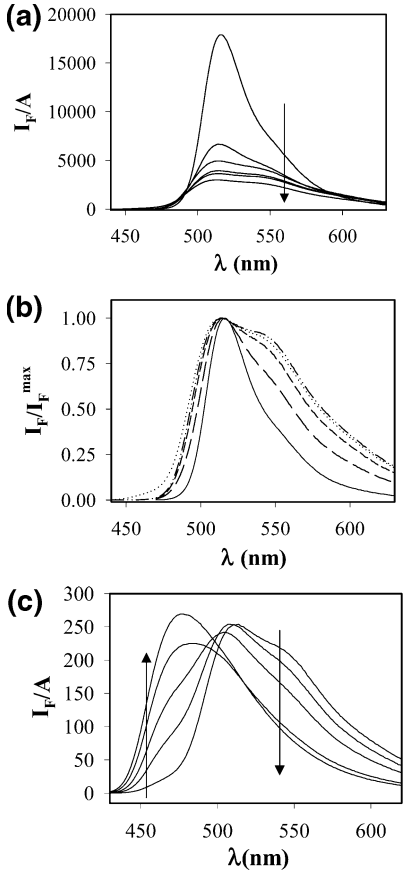

Figure 5. (a) Steady-state emission spectra (λ^{ex} = 424 nm), normalized by the absorbance, of 5.0 × 10^{-6} M OG488 aqueous solutions at pH values 11.65, 4.68, 3.44, 2.12, 1.26, and [$HClO_4$] = 2 M. Arrow indicates the decrease in pH value. (b) Spectra of (a) normalized at the maximum; pH 11.65 (—), 4.68 (− − −), 3.44 (- - -), 1.26 (- ••), and [$HClO_4$] = 2 M (•••). The spectrum at pH 2.12 has been removed for clarity. (c) Steady-state emission spectra (λ^{ex} = 424 nm), normalized by the absorbance, of 5.0 × 10^{-6} M OG488 aqueous solutions at [$HClO_4$] = 3.0, 5.0, 6.0, 8.0, and 9.5 M. Arrows indicate the increase in $HClO_4$ concentration.

We also performed a quantitative study of steady-state fluorescence emission. The emission intensity versus pH was recorded at four excitation wavelengths (420, 440, 460, and 480 nm) and two emission wavelengths (515 and 550 nm). The variations in intensity with changes in pH above 4 were in good agreement with changes in absorption spectra. Thus, fluorescence intensity versus pH curves showed the ground-state monoanion−dianion pK_a (i.e., pK_M). On the contrary, changes in intensity below pH 4 did not correspond to changes in absorption spectra. This feature might indicate the presence of an excited-state proton transfer (ESPT) between neutral and monoanionic species. Taking into account the assumptions that (1) every excited cation rapidly deprotonates to excited neutral form, (2) under steady-state conditions the species concentration ratio depends on pH and is determined by an apparent excited-state pK_N*, and (3) there is no excited-state proton exchange between monoanion and dianion, the following equation can be derived:[6]

$$I_F = (\epsilon_C\alpha_C + \epsilon_N\alpha_N + \epsilon_M\alpha_M) \times \left[\frac{\phi_N}{1 + 10^{pH-pK_N^*}} + \frac{\phi_M}{1 + 10^{pK_N^*-pH}}\right] + \phi_D\epsilon_D\alpha_D \quad (21)$$

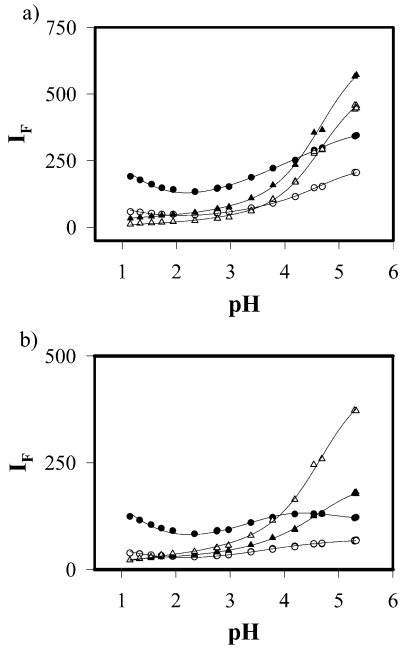

Figure 6. Global fitting of I_F vs pH according to eq 21: $\lambda^{ex} = 420$ (●), 440 (○), 460 (▲), and 480 nm (△); $\lambda^{em} = 515$ (a) and 550 nm (b).

Here, ϵ_i indicates the absorption coefficient of the *i*th species at the excitation wavelength, α_i is the ground-state molar fraction of the *i*th species at each pH, ϕ_i are adjustable parameters related to the *i*th form fluorescence quantum yields, and pK_N* indicates an apparent excited-state neutral/monoanion acid−base equilibrium constant.

We fitted globally I_F versus pH (between pH 1 and 5), using the four excitation wavelengths and the two different emission wavelengths, through a nonlinear least-squares method based on Marquardt's algorithm. Absorption coefficients ϵ_i and molar fractions α_i were known parameters, using values recovered in the previous section. The ϕ_i were local adjustable parameters, while pK_N* was linked over all the curves. Figure 6 shows the fitting results (global r^2 was 0.9983). The recovered pK_N* value was 2.67 ± 0.06.

In summary, in excited OG488, we found that the cationic form turned to a super-photoacid, and a 1 unit decrease in pK_a between neutral and monoanion was obtained through fluorescence intensity versus pH fitting. On the contrary, the dianionic form seemed not to be involved in any ESPT reaction on the time scale of the excited-state decay time of this species, since fluorescence intensity at pH values above 5 varied according to the changes in absorbance.

Effect of the HOAc/OAc⁻ Buffer Species in the Excited-State Behavior of OG488. *Absorption and Steady-State Fluorescence Measurements.* To ensure the absence of ground-state reactions between acetate/acetic acid and the prototropic species of OG488, we recorded the absorption spectra of solutions of OG488 at a particular pH, increasing the total buffer concentration between 0 and 1.5 M. We did this for solutions at pH 2.93, 4.00, 4.30, 4.60, and 9.00. The absorption spectra of the solutions at each pH were coincident with the corresponding spectra at the same pH value in the absence of buffer. Only slight effects, presumably because of ionic strength changes, were found. Hence, the acetate buffer does not alter the ground-state equilibria of OG488.

With regard to steady-state fluorescence spectra, the emission spectrum of the monoanion shows a maximum at 513 nm and a shoulder around 550 nm. The emission spectrum of the dianion shows a maximum at 515 nm. The emission efficiency is much higher for the dianion than for the monoanion. In Figure 7, the steady-state fluorescence spectra from aqueous OG488 solutions in the presence of increasing buffer concentrations at the same pH (4.3) are shown. The excitation wavelength was 420 nm. As can be seen, an increase in the buffer concentration resulted in a pronounced increase in emission intensity. The inset in Figure 7 shows variations in emission spectra at 515 nm with buffer concentration increase, at $\lambda^{ex} = 420$ nm and at pH 4.0, 4.3, and 4.6. At these pH values and excitation wavelength, the monoanion promotes to the excited-state preferentially. Since the 515 nm emission is dominated by dianion emission, these results indicate that increasing the total buffer concentration C^{buff} increases the concentration of excited dianion molecules. Thus, under these conditions, the excited monoanion is converted to the dianion during its lifetime. Similar behavior was found in fluorescein with phosphate buffer[6,7] and *N*-acetyl aspartic acid.[8]

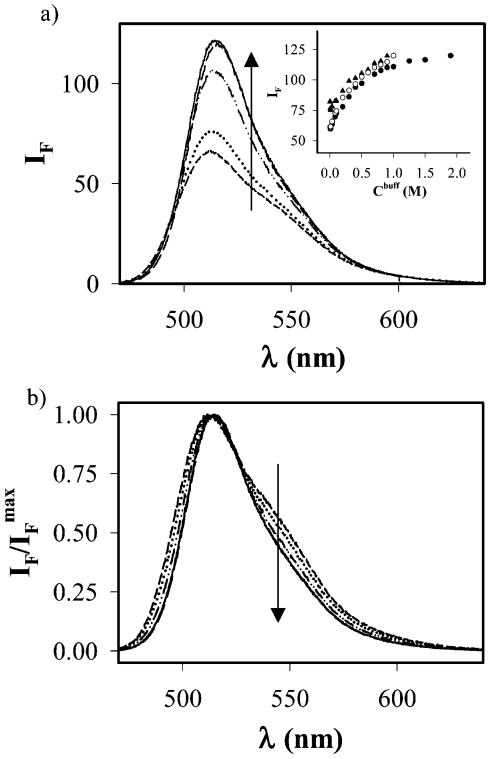

Figure 7. (a) Steady-state emission spectra ($\lambda^{ex} = 420$ nm) of 2.5 × 10^{-6} M OG488 aqueous solutions at pH 4.30 in the presence of acetate buffer at $C^{buff} = 5 \times 10^{-3}$ (- - -), 8×10^{-2} (···), 0.5 (- ··), 1.0 (—), and 1.5 M (— — —). (b) Spectra of (a) normalized at the maximum. Arrows indicate the increase in buffer concentration. Inset: increase in steady-state fluorescence intensity ($\lambda^{ex} = 420$ nm, $\lambda^{em} = 515$ nm) with increasing buffer concentration at pH values 4.0 (▲), 4.3 (●), and 4.6 (○).

We also compared, in Figure 8, fluorescence intensity versus pH curves in 1 M acetate buffered media and in the absence of buffer. As can be seen in this figure, fluorescence intensity showed a higher increase at lower pH values in the presence of buffer compared to the fluorescence intensity in the absence of buffer. Furthermore, in the presence of buffer, a decrease in intensity is noticed at pH values above 5.

These features indicate the presence of excited-state proton reactions promoted by the buffer species. Under these conditions, the fluorescence intensity does not depend on which form is excited preferentially, since the rapid proton-transfer reaction in the excited-state erases all effects due to preferential excitation

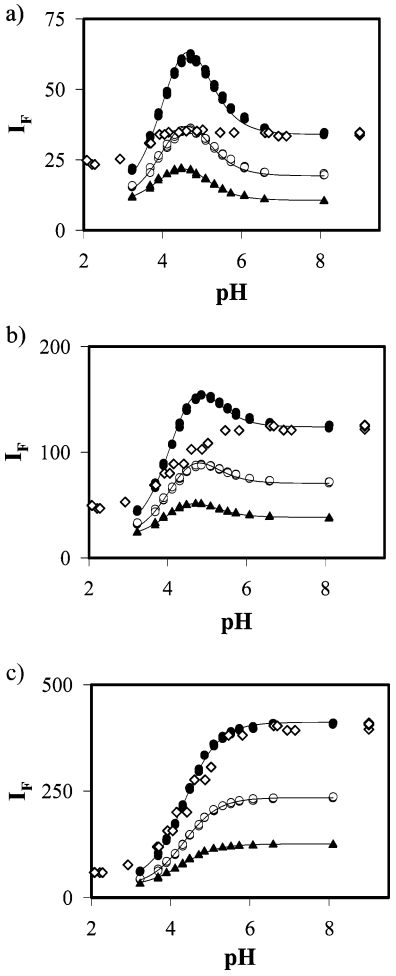

Figure 8. Emission intensity vs pH of 2.5×10^{-6} M OG488 aqueous solutions in the presence of 1 M acetate buffer: $\lambda^{ex} = 420$ (a), 440 (b), and 460 nm (c), and $\lambda^{em} = 500$ (○), 515 (●), and 550 nm (▲). For comparison, intensity of solutions in the absence of buffer at $\lambda^{em} =$ 515 nm are also shown (◇). Solid lines represent the global fitting according to eq 22.

of any one form. For this model we can express the normalized fluorescence intensity by[6]

$$\frac{I_F}{A} = \frac{\phi_M}{1 + 10^{(pH - pK_M^*)}} + \frac{\phi_D}{1 + 10^{(pK_M^* - pH)}} \qquad (22)$$

where I_F/A is the fluorescence intensity at λ^{em}, normalized by absorbance at the excitation wavelength, ϕ_M and ϕ_D are adjustable parameters directly related to the relative fluorescence efficiencies of the mono- and dianion at λ^{em}, and pK_M^* is an apparent pK_a for the excited-state proton reaction $M^* \leftrightarrows D^* + H^+$. We recorded titration curves of fluorescence intensity, normalized by absorbance, versus pH of solutions of OG488 in the presence of 1 M acetate buffer. Excitation wavelengths were 420, 440, and 460 nm, while emission was recorded at 500, 515, and 550 nm. We globally fitted these curves, according to eq 22 through a nonlinear least-squares method based on Marquardt's algorithm, using pK_M^* as a shared (i.e., linked) parameter over each curve and ϕ_M and ϕ_D as local fitting parameters. In Figure 8, the fitting process results are shown. The average values of the ratios ϕ_D/ϕ_M at emission wavelengths of 500, 515, and 550 nm were 4.3 ± 0.5, 5.2 ± 0.6, and 2.5 ± 0.2, respectively. These ratios give an idea of the higher fluorescence efficiency of the dianionic form over the monoanion form. Global r^2 of the fitting was 0.9985. We recovered a

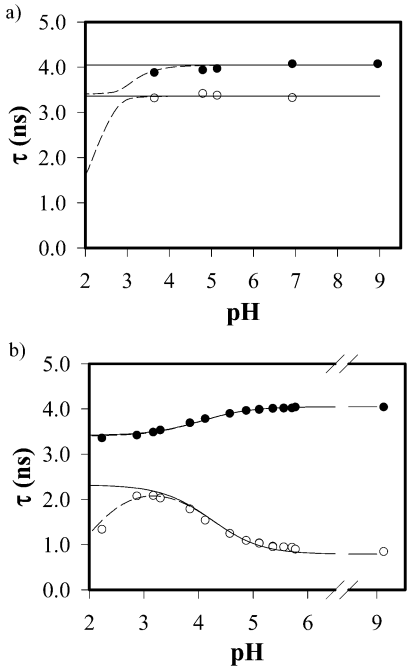

Figure 9. Decay times, in the absence (a) and the presence (b) of 1 M acetate buffer, estimated by global biexponential analyses (symbols) and calculated using the rate constant values recovered from the global compartmental analysis (solid lines), with $k_{MD} = 0$. The decay times calculated using the rate constant values of Table 3 and the estimated value of k_{MD} (3.7×10^{10} M^{-1} s^{-1}) are also shown as dashed lines.

pK_M^* value of 4.42 ± 0.01 with a dependency coefficient of 0.824. This indicates the acceptable independency of the recovered value. The recovered value is slightly lower compared to the ground-state pK_a value (4.69−4.8[2]).

Time-Resolved Fluorescence Measurements. Global Analyses. Standard global analyses (in terms of τ_i and p_i from eq 9) were performed on fluorescence decay traces of OG488 solutions in the absence of buffer and in the presence of 1 M acetate buffer, over a pH range between 2.12 and 9.12. The excitation wavelength was 420 nm, which produces preferential monoanion/neutral excitation. Emission wavelengths were 490, 515, 525, 550, 570, 580, and 600 nm. In these analyses, decay times τ_i can be linked, while pre-exponential factors p_i must be different at every emission wavelength.

We note that a different behavior is found whether acetate buffer is added or not. In the absence of buffer, decay traces were biexponential. Two decay times were recovered as represented in Figure 9a, with both pre-exponential factors being positive (represented as symbols in Figure 10a,b). The decay times τ_i were pH independent above pH 4.79, while below this value the longer decay time slightly decreased with lower pH values. To confirm this, we fitted globally all the decay traces in the absence of buffer with the decay times linked over every trace. Only decay traces within the pH range 4.79−8.95 were well fitted with two decay times: 4.04 and 3.39 ns. On the contrary, decay traces at pH values below 4.79 introduced in the global analysis did not fit properly. This clearly indicated variations in the decay times at pH values below 4.79. At pH values above 6.92, only the dianionic form is present, and the decay trace became monoexponential. The decay time (4.04 ± 0.06 ns) in this pH range corresponds to the dianion lifetime. The shorter decay time might represent monoanion lifetime ($\tau_M = 1/k_{0M}$), supposing the absence of excited-state deprotonation ($M^* \rightarrow D^*$) or the sum of monoanion decay rate constant and excited-state deprotonation rate constant ($\tau = 1/(k_{0M} + k_{DM})$)

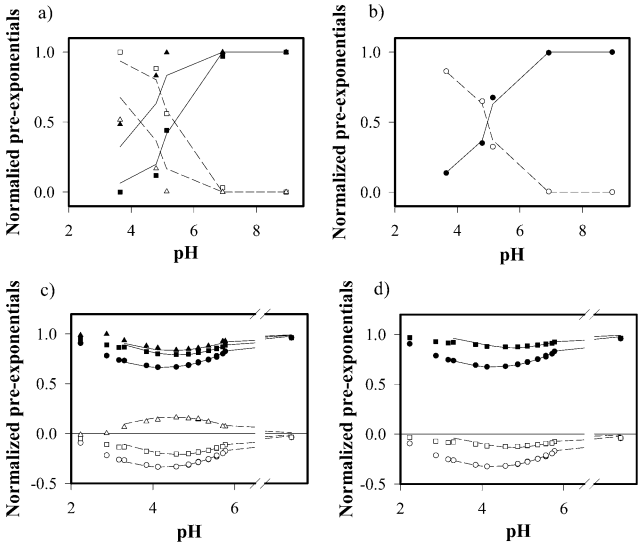

Figure 10. Normalized pre-exponential factors p_i recovered from global analyses (symbols), and calculated with results from global compartmental analysis (lines), using the parameters of Table 3 and the recovered $\tilde{b}_i$ and $\tilde{c}_i$ values. Pre-exponentials associated with the longer decay time are represented with solid lines and filled symbols, while factors associated with the shorter decay time are represented with dashed lines and unfilled symbols. (a) Decays of solutions in the absence of acetate buffer, with $\lambda^{ex} = 420$ nm and $\lambda^{em} = 515$ nm (▲ and △) and 580 nm (■ and □). (b) Decays of solutions in the absence of acetate buffer, with $\lambda^{ex} = 420$ nm and $\lambda^{em} = 550$ nm (● and ○). (c) Decays of solutions in the presence of 1 M acetate buffer, with $\lambda^{ex} = 420$ nm and $\lambda^{em} = 515$ nm (● and ○), 550 nm (■ and □), and 600 nm (▲ and △). (d) Decays of solutions in the presence of 1 M acetate buffer, with $\lambda^{ex} = 420$ nm and $\lambda^{em} = 525$ nm (● and ○) and 570 nm (■ and □).

when excited-state deprotonation exists. In the absence of added buffer, values of the individual rate constants k_{0M} and k_{DM} cannot be determined; only their sum can be recovered. Hence, these two situations are indistinguishable according to identifiability studies.[17,29]

Global analyses of decay traces from samples in the presence of 1 M acetate buffer showed biexponential decay laws. In contrast to traces in the absence of buffer, the decay times are clearly pH-dependent, and the shorter decay time showed a negative pre-exponential. These are characteristic features of an excited-state proton transfer. As steady-state results suggest, the acetate buffer may act as a suitable proton acceptor or donor, resulting in a reversible excited-state reaction. Figure 9b represents the decay times. The associated pre-exponential factors are plotted as symbols in Figure 10c,d. The short decay time is usually a rise-time, since formation of D* from M* in the excited-state leads to an increase in emission. But this does not happen at the 600 nm emission wavelength. At this λ^{em}, monoanion emission is higher than that of dianion. Thus, the ESPT M*→D* produces a loss in emission at 600 nm. This is indicated as a positive pre-exponential factor associated with the shorter decay time at this emission wavelength.

Time-Resolved Fluorescence Measurements. Global Compartmental Analysis. The recovered decay times from standard global analyses are closely connected to the underlying rate constants. Traditional two-step approaches have used these results to recover the rate constant values through several graphical or numerical methods. We used the powerful global compartmental analysis method for solving the excited-state kinetics of OG488 in the presence of acetate buffer. Global compartmental analysis takes advantage of the relationship between different decay traces over the complete fluorescence decay surface. Thus, rate constants and spectral parameters are recovered through a single-step method directly from the decay data.

TABLE 3: Recovered Rate Constant Values from Global Compartmental Analysis of the Fluorescence Decay Surface of OG488 Aqueous Solutions at pH between 3.30 and 9.12, in the Absence and the Presence of 1 M Acetate Buffer

k_{0M} (s^{-1})	$(2.94 \pm 0.01) \times 10^8$	
k_{0D} (s^{-1})	$(2.47 \pm 0.01) \times 10^8$	
k_{MD} (M^{-1} s^{-1})	0[a] or 3.7×10^{10} [c]	
k_{DM} (s^{-1})	$(3.57 \pm 0.15) \times 10^6$	
k^b_{MD} (M^{-1} s^{-1})	$(1.79 \pm 0.01) \times 10^8$	
k^b_{DM} (M^{-1} s^{-1})	$(9.70 \pm 0.02) \times 10^8$	$pK_M^* = 4.022 \pm 0.003$[d]

[a] Kept fixed to zero during the fitting process. [c] Calculated using $k_{DM} = 3.57 \times 10^6$, $pK_M^* = 4.022$, and eq 26. [d] Calculated using eq 25.

The fluorescence decay surface introduced in the fitting program included decays in the presence and in the absence of buffer. According to the identifiability study,[17] this fluorescence decay surface obeys the identifiability conditions on rate constants, since k_{0D} is known through high pH decay traces, and the sum ($k_{0M} + k_{DM}$) can be determined through decays in the absence of proton acceptor or donor. These conditions allow one to uniquely obtain the rest of the rate constant values from decays at a single nonzero buffer concentration. If k_{0D} and ($k_{0M} + k_{DM}$) could not be distinguished, decays at two different buffer concentrations would be required.[17] For the global compartmental analysis, the complete fluorescence decay surface included 70 decay traces due to excitation at a single wavelength (420 nm): 50 decays corresponded to ten pH values (between 9.12 and 3.30), at 1 M total buffer concentration, at 515, 525, 550, 570, and 600 nm emission wavelengths (all recorded at 5.94 ps/channel); eight decay traces were recorded from four OG488 solutions at different pH values (5.11−5.77) and 1 M buffer concentration, at 515 and 525 nm emission wavelengths and 2.46 ps/channel. Finally, the surface included 12 decays of solutions without added buffer, at four pH values (3.64−8.95), at 515, 550, and 580 nm emission wavelengths and 5.94 ps/channel. The adjustable parameters linking scheme is shown in Scheme 3. The rate constants k_{0i} and k_{ij} were linked over the complete fluorescence decay surface. The rate constants k^b_{DM} and k^b_{MD} were linked over decays in the presence of buffer, whereas they were kept fixed to zero for decays in the absence of buffer (see linking configuration shown in Scheme 3). Excitation spectral parameters, $\tilde{b}_M$(pH, λ^{ex}), were linked at the same pH (only one excitation wavelength was used), and emission spectral parameters, $\tilde{c}_M(\lambda^{em})$, were linked in decays at the same emission wavelength.

In the various global compartmental analyses performed, k_{MD} always tended toward zero. This was due to the noncompetitive excited-state reprotonation rate at the considered pH range ($[H^+]$ is between 5.0×10^{-4} and 7.6×10^{-10} M). Thus, in the definitive analysis k_{MD} was kept fixed to zero. The recovered rate constant values from this global compartmental analysis are shown in Table 3. The global reduced χ^2 value for this fitting was 1.150. Visualization of weighted residuals and autocorrelation functions were also used as goodness-of-fit criteria. The recovered dianion lifetime ($\tau_D = 4.05 \pm 0.02$ ns) was in perfect agreement with the decay time obtained from monoexponential decay traces in the absence of buffer at high pH. In Figure 11, we show some representative decay traces, the fitted functions from the global compartmental analysis, the weighted residuals plots, and the autocorrelation function graphs.

Using the k_{ij} values of Table 3, the pK_a value for acetate buffer ($pK_a^{buff} = 4.756$),[30] and the total buffer concentration C^{buff} (0

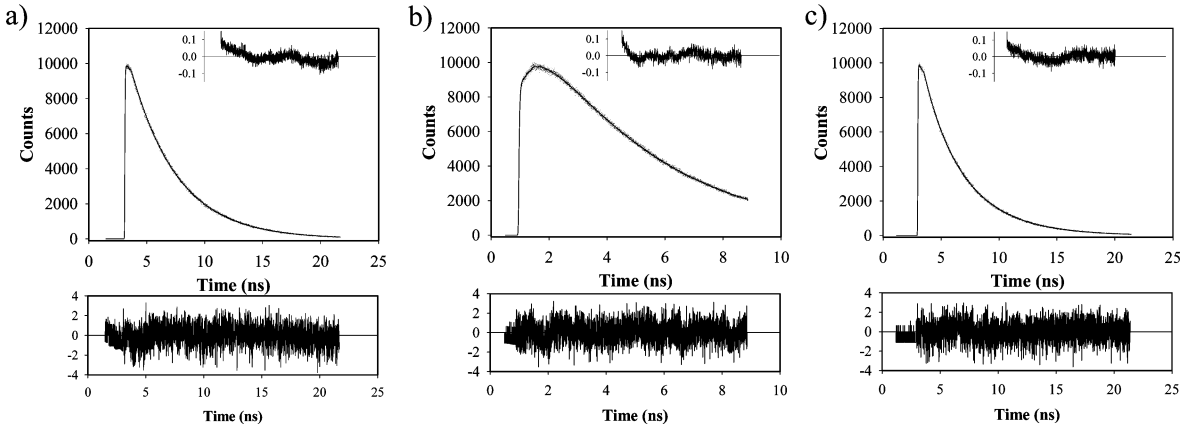

Figure 11. Representative fluorescence decay traces, fitted by global compartmental analysis, of OG488 5×10^{-6} M aqueous solutions: (a) $C^{buff} = 0$, pH = 5.13, $\lambda^{ex} = 420$ nm, $\lambda^{em} = 515$ nm, and a time scale of 5.94 ps/channel; (b) $C^{buff} = 1$ M, pH = 5.36, $\lambda^{ex} = 420$ nm, $\lambda^{em} = 515$ nm, and a time scale of 2.46 ps/channel; (c) $C^{buff} = 1$ M, pH = 4.12, $\lambda^{ex} = 420$ nm, $\lambda^{em} = 600$ nm, and a time scale of 5.94 ps/channel. In the figure, the experimental decay trace, the fitted function (lines), the weighted residuals (lower graph), and the autocorrelation functions (insets) are shown. The instrument response function is not plotted for clarity.

and 1 M) used, we calculated $\tau_{1,2}$ according to eqs 10 and 11 for the pH range used in this study. Figure 9b shows the plot of $\tau_{1,2}$ values versus pH for decays at 1 M acetate buffer. Calculated decay times are plotted as solid lines, while the symbols in Figure 9b are the $\tau_{1,2}$ values recovered from the standard global biexponential analyses of decays in the presence of buffer. Figure 9a shows the calculated decay times (solid lines) for decays in the absence of buffer according to results in Table 3 and the recovered decay times from global biexponential analyses. The agreement between the decay times $\tau_{1,2}$ from global compartmental and global biexponential analyses is excellent at pH values 3.30 and above. At pH values below 3.30 in the presence of 1 M acetate buffer, the shorter decay time recovered by global analysis was appreciably lower than the calculated one. This is due to the higher $[H^+]$ value in this pH range, which makes the reprotonation of the dianion ($k_{MD} \times [H^+]$) not negligible anymore. Consequently, the assumption made that $k_{MD} = 0$ in the global compartmental analysis is not correct at pH values below 3.30.

Figure 12 shows the values of the excitation, $\tilde{b}_i$, and emission parameters, $\tilde{c}_i$, recovered from the global compartmental analysis. Some additional considerations should be made, since the OG488 neutral form is present upon excitation at 420 nm and at pH values between 3.30 and 5.00. According to absorption, steady-state fluorescence, and acid−base properties of OG488, there are three prototropic species involved at the pH range studied (N, M, and D). Nevertheless, as has been demonstrated, the ESPT between M* and D* promoted by acetate buffer species is well described by a two-state excited-state model. The influence of the neutral form might be a point of interest within this study. Through steady-state fluorescence measurements we found an excited-state proton transfer between N* and M* in buffer-free conditions. This behavior was also found in fluorescein N* and M* species.[22] If this process is assumed, both species, N* and M*, rapidly interconvert. Besides, the presence of HOAc and OAc^- species (mainly HOAc in the pH range in which the neutral form might have an effect) could promote and accelerate the N* ⇆ M* transformation. Definition of the compartments as a subsystem of species acting in a unique kinetic way is the key to understand the apparent "disappearance" of the neutral form. While N* ⇆ M* interconversion is rapid enough, the limiting kinetic factor of the system would be transformation toward D*. Hence, N* and M* could act as a single compartment. Therefore, excitation parameters, $\tilde{b}_i$, show

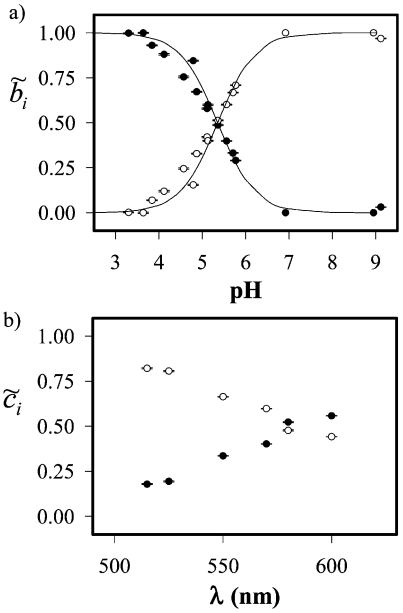

Figure 12. Plots of the excitation $\tilde{b}_i$ (a) and emission $\tilde{c}_i$ (b) parameter values recovered by global compartmental analysis for the dianion (○) and neutral/monoanion (●) compartments. The errors are represented within the symbols. Calculated values for excitation parameters, according to eq 23, are also shown as lines.

a typical two-species profile. Thus, we calculated the excitation parameter, $\tilde{b}_M$, according to absorption results and the previously determined pK_a values, using eq 23:

$$\tilde{b}_M = \frac{\epsilon_N \alpha_N + \epsilon_M \alpha_M}{\epsilon_N \alpha_N + \epsilon_M \alpha_M + \epsilon_D \alpha_D} \qquad (23)$$

This equation includes the excitation contribution of both neutral and monoanionic forms in one single compartment.

Figure 12 shows the good agreement between the $\tilde{b}_i$ values recovered by global compartmental analysis and those calculated using eq 23. Furthermore, $\tilde{c}_i$ values coincided very well with the steady-state fluorescence of OG488. The dianion emits preferentially at 515 and 525 nm, while the shoulder in the monoanion emission spectrum produces a higher contribution at 570 nm. The monoanion even shows a higher quantum yield at 600 nm than the dianion. This is also obtained by global compartmental analysis, since $\tilde{c}_M(600\text{ nm}) > 0.5$. In addition,

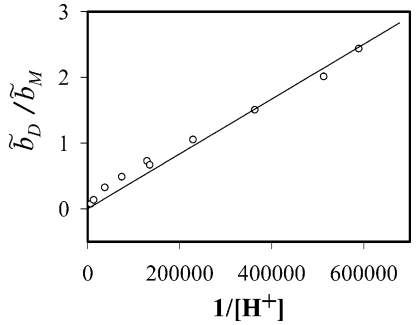

Figure 13. Linear fitting of the ratio of the recovered excitation parameters $\tilde{b}_D/\tilde{b}_M$ vs $1/[H^+]$ according to eq 24.

one can compare, in a more quantitative treatment, the ratio $\tilde{c}_D/\tilde{c}_M$ with the given ϕ_D/ϕ_M from the steady-state fluorescence section. These two ratios are closely related and give an idea of the agreement between the different methods. The results obtained in the steady-state fluorescence for ϕ_D/ϕ_M were 5.2 at $\lambda^{em} = 515$ nm and 2.5 at $\lambda^{em} = 550$ nm, whereas the $\tilde{c}_D/\tilde{c}_M$ ratios from the global compartmental analysis were 4.6 and 2.0 at the emission wavelengths 515 and 550 nm, respectively. The two sets of ratios are in good agreement, and they are indicative of the higher quantum yield of the dianion at 515 nm and the shoulder at 550 nm of the monoanion spectrum that produces a lower value of the ratios.

Furthermore, $\tilde{b}_i$ values provide quantitative information about ground-state equilibria. Assuming only contributions from monoanion and dianion, we have

$$\frac{\tilde{b}_D}{\tilde{b}_M} = \frac{K_M}{\epsilon_R[H^+]} \tag{24}$$

where $\epsilon_R = \epsilon_M/\epsilon_D$ is the ratio of absorption coefficients at the excitation wavelength. From our absorption results, this relative absorption coefficient is 4.519 at 420 nm. Equation 24 allows one to calculate the ground-state constant, K_M, from monoanion−dianion equilibrium. The linear fitting of $\tilde{b}_D/\tilde{b}_M$ versus $1/[H^+]$ is shown in Figure 13. The slope of the linear fit was $(4.17 \pm 0.14) \times 10^{-6}$. This value together with known ϵ_R provided a pK_M value of 4.72 ± 0.01, which is in excellent agreement with other calculated values for the M ⇆ D ground-state equilibrium (4.69−4.8[2]).

In addition, k^b_{DM} and k^b_{MD} can provide the value of the excited-state K_a* according to eq 25:

$$pK_a^* = \log(k^b_{DM}) - \log(k^b_{MD}) + pK_a^{buff} \tag{25}$$

Using the recovered k^b_{DM} and k^b_{MD} values and the pK_a^{buff} value of acetic acid, we obtained pK_a* $= 4.022 \pm 0.003$. This value represents a decrease with respect to that recovered from steady-state data (4.42 ± 0.01). Since the pK_a* $= 4.022$ has been calculated from the kinetic constants, this represents the actual pK_a*, while the steady-state value is an apparent pK_a*, according to the assumptions in eq 22.

Assuming this pK_a* (4.022) and the recovered k_{DM}, the value for k_{MD} can be estimated using eq 26:

$$K_a^* = \frac{k_{DM}}{k_{MD}} \tag{26}$$

This resulted in a k_{MD} value of 3.7×10^{10} M^{-1} s^{-1}. This is a typical value for a diffusion controlled rate,[31] as expected for a reprotonation reaction. Using this k_{MD} value (instead of zero) and the rate constant values of Table 3, we recalculated the decay times. Parts a and b of Figure 9 (dashed lines) show these calculated decay times in the absence and presence of buffer, respectively. An excellent agreement was found between these calculated decay times and those from global biexponential analyses, including pH values below the lowest value used in the global compartmental analysis, 3.30.

TABLE 4: Rate Constant Values Recovered from Global Compartmental Analysis of the Fluorescence Decay Surface of OG488 Aqueous Solutions at pH between 3.30 and 9.12, in the Absence and the Presence of 1 M Acetate Buffer, Including the Ionic Strength Effects

k_{0M} (s^{-1})	$(2.90 \pm 0.01) \times 10^8$	
k_{0D} (s^{-1})	$(2.48 \pm 0.01) \times 10^8$	
k_{MD} (M^{-1} s^{-1})	0[a]	
k_{DM} (s^{-1})	$(4.3 \pm 0.2) \times 10^6$	
k^b_{MD} (M^{-1} s^{-1})	$(2.05 \pm 0.01) \times 10^8$	
k^b_{DM} (M^{-1} s^{-1})	$(8.87 \pm 0.02) \times 10^8$	pK_M* $= 4.120 \pm 0.003$[c]

[a] Kept fixed to zero during the fitting process. [c] Calculated using eq 25.

Finally, the pre-exponential factors were also calculated with recovered k_{ij}, $\tilde{b}_i$, and $\tilde{c}_i$, using eqs 12 and 13. Figure 10 shows the calculated factors and pre-exponentials from global analyses of decay traces in the absence (Figure 10a,b) and presence (Figure 10c,d) of 1 M acetate buffer. As can be seen in Figure 10, a good agreement was found between calculated pre-exponentials and the factors recovered from global biexponential analyses.

Influence of the Ionic Strength. For simplicity, in the previous section we have not considered the ionic strength effects in the equations derived from the model. In this section, we develop a simple approach introducing the activity coefficients into the Henderson−Hasselbach equation to relate the $[H^+]$ and the sodium acetate concentration with pH and activity. Furthermore, the primary kinetic salt effect on the rate constants has also been considered.

Taking into account the activity coefficients for sodium acetate in the concentration range 0.1−1 M[30] and neglecting the ionic strength from other ionic species at very low concentration, we calculated $[H^+]$ and the buffer species concentrations, at the different pH values studied. Using these corrected concentrations, we performed a new global compartmental analysis with the same experimental decay traces used in the previous section. Table 4 shows the recovered rate constants from this new analysis. The spectral parameters, $\tilde{b}_i$ and $\tilde{c}_i$, were the same as those represented in Figure 9, within the experimental error. The global χ^2 value for this fitting was 1.097, better than that previously obtained.

Introducing in eqs 10 and 11 the mean ionic activity coefficient, $\gamma_\pm$, and using the k_{ij} values of Table 4 and the other pertinent parameters, we calculated the decay times. For this, we have obtained a semiempirical function based on Davies' equation to relate $\gamma_\pm$ and sodium acetate ionic strength, I, in the range 0.1−1 M.

$$\log \gamma_\pm = -0.51\left(\frac{\sqrt{I}}{1+\sqrt{I}} - LI + QI^2\right) \tag{27}$$

where L and Q are two adjustable parameters. We fitted this equation to the experimental data of $\gamma_\pm$ from ref 30 resulting in $L = 0.40 \pm 0.01$ and $Q = 0.11 \pm 0.02$. This rough approach represents well the experimental sodium acetate $\gamma_\pm$ in the range of ionic strength studied.

Figure 14 shows the plot of $\tau_{1,2}$ values versus $-\log [H^+]$ for decays at 1 M acetate buffer. Calculated decay times are plotted

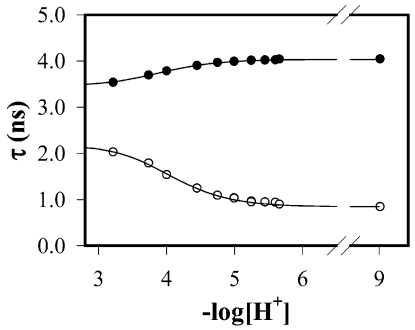

Figure 14. Decay times in the presence of 1 M acetate buffer, estimated by global biexponential analyses (symbols) and calculated using the rate constant values of Table 4, including the ionic strength effects within the general equations (solid lines).

as solid lines, while the symbols are the $\tau_{1,2}$ values recovered from the standard global biexponential analyses. The agreement between the decay times, $\tau_{1,2}$, from global compartmental and global biexponential analyses is excellent. Comparing Figures 9b and 14, we note that both are essentially the same, although $-\log[H^+]$ is around 0.1 unit lower than the pH.

We have also considered the primary kinetic salt effect on k^b_{DM}. Since k_{MD} was kept to zero in the fitting and k^b_{MD} and k_{DM} characterize reactions involving uncharged species, this effect does not alter these rate constants. Applying eq 27 to the well-known equation of the primary kinetic salt effect resulted in a variation of this constant due to variations in ionic strength which is only slightly higher than the associated error recovered for k^b_{DM} in the global compartmental analysis. Since the range of variation of k^b_{DM} is not noteworthy and the global compartmental analysis results in excellent statistical parameters and yields kinetic and spectral parameters (averaged by the overall surface of the experimental data) that simulate very well the experimental decay times and pre-exponentials, we concluded that the single value for the rate constant k^b_{DM} provided represents well the characteristic deprotonation rate of OG488 monoanion mediated by acetate anion.

Discussion

In this paper, we have provided valuable basic information about the fluorescent pH indicator 2′,7′-difluorofluorescein, OG488. A complete absorption study, including acid−base equilibria, determination of ground-state pK_a values, and recovery of molar absorption coefficients of every prototropic species, has been performed. Four prototropic species were described: cation, neutral, monoanion, and dianion. We also provided absorption and NMR evidence for the existence of three tautomers in neutral species: quinoid, zwitterionic, and lactonic.

We also performed a fluorimetric study of aqueous solutions of OG488. Emission spectra of the different prototropic forms were described. The cationic form, acting as a super-photoacid upon photoexcitation, showed an emission spectrum only detected at extreme acidic concentrations. We also did global nonlinear least-squares fitting of the steady-state fluorescence intensity variations with pH. We assumed, based on steady-state fluorescence data, that (a) all excited cation molecules rapidly deprotonate to neutral, (b) there is no excited-state proton-transfer reaction between monoanion and dianion on the time scale of the excited-state lifetime of these species, and (c) ESPT between neutral and monoanionic excited species is rapid enough to occur during their lifetimes. Thus, we recovered the pK_N* = 2.67 ± 0.06.

We have also demonstrated that HOAc/OAc$^-$ is a suitable proton donor/acceptor in the ESPT between OG488 monoanion and dianion. Acetate buffer does not alter OG488 ground-state equilibria. Using steady-state fluorescence, we have shown that an increase in buffer concentration produces a higher dianionic contribution to emission when preferential excitation of the monoanion is used. A steady-state fluorescence methodology was used to calculate an apparent pK_a* value, assuming a rapid ESPT promoted by the proton acceptor or donor. Steady-state fluorescence data were fitted through a nonlinear least-squares process.

Time-resolved fluorescence showed biexponential decays for decays at 1 M acetate buffer and in the absence of buffer. Global analyses of decays of solutions without added buffer showed two decay times whose associated pre-exponentials were positive. Decays of solutions of OG488 in 1 M buffered media showed two pH-dependent decay times, of which the shorter time is a rise-time (negative pre-exponential at emission wavelengths between 490 and 570 nm). The presence of a pH-dependent rise-time is clear evidence of an excited-state proton transfer.

Kinetics of ESPT has been solved through global compartmental analysis. The simultaneous fitting of a fluorescence decay surface, formed with decays in the absence and presence of 1 M acetate buffer, and the observation of monoexponential decays at very high pH provide identifiability conditions on all pertinent rate constants.[17] The recovered rate constants and spectral parameters, $\tilde{b}_i$ and $\tilde{c}_i$, allow one to calculate the decay times and pre-exponential factors. The results from global compartmental analysis showed excellent agreement with standard global analyses results (in terms of decay times, τ_i, and pre-exponentials, p_i, eq 9), absorption measurements (excellent match between recovered and experimental $\tilde{b}_i$ values), and fluorescence emission data (qualitative agreement between $\tilde{c}_i$ values and the fluorescence emission spectra).

We also emphasize the definition of a compartment as a subset of species acting kinetically in a unique way. Thus, it has been shown that neutral and monoanion species behave as a single compartment because of the sufficiently rapid interconversion between each species during their excited-state lifetime and the same emissive behavior (quinoid configurations in the xanthene moiety) of both species. Although three prototropic forms are present in the ground and excited states (neutral, monoanion, and dianion) in the considered pH range (2.12−9.12), the ESPT process can be completely described by a two-state excited-state model.

We have also demonstrated that ionic strength effects are very small when the proton acceptor/donor is sodium acetate/acetic acid (electrolyte 1:1). Therefore, the approach in which we neglect ionic strength effects is valid when the buffer concentration range is between 0 and 1 M of a 1:1 electrolyte.

Acknowledgment. A.O. thanks the Spanish Ministry of Education, Culture, and Sports for a Ph.D. fellowship and the travel grants to the K. U. Leuven and I.T.Q.B. (Oeiras). He also is thankful for the hospitality during his stays. This work was supported by Grant BQU2002-01311 from the Spanish Ministry of Science and Technology.

References and Notes

(1) Haugland, R. P. *Handbook of Fluorescent Probes and Research Products*, 9th ed.; Molecular Probes, Inc., Eugene, OR, 2002.

(2) Sun, W.; Gee, K. R.; Klaubert, D. H.; Haugland, R. P. *J. Org. Chem.* **1997**, *62*, 6469−6475.

(3) Thomas, D.; Tovey, S. C.; Collins, T. J.; Bootman, M. D.; Berridge, M. J.; Li, P. *Cell Calcium* **2000**, *28*, 213−223.

(4) Goodnough, M. C.; Oyler, G.; Fishman, P. S.; Johnson, E. A.; Neale, E. A.; Keller, J. E.; Te, W. H.; Clark, M.; Hartz, S.; Adler, M. *FEBS Lett.* **2002**, *513*, 163−168.

(5) Rusinova, E.; Tretyachenko-Ladokhina, V.; Vele, O. E.; Senear, D. F.; Alexander Ross, J. B. *Anal. Biochem.* **2002**, *308*, 18−25.

(6) Yguerabide, J.; Talavera, E.; Alvarez-Pez, J. M.; Quintero, B. *Photochem. Photobiol.* **1994**, *60*, 435−441.

(7) Alvarez-Pez, J. M.; Ballesteros, L.; Talavera, E.; Yguerabide, J. *J. Phys. Chem. A* **2001**, *105*, 6320−6332.

(8) Crovetto, L.; Orte, A.; Talavera, E. M.; Alvarez-Pez, J. M.; Cotlet, M.; Thielemans, J.; De Schryver, F. C.; Boens, N. *J. Phys. Chem. B* **2004**, *108*, 6082−6092.

(9) Orte, A.; Crovetto, L.; Bermejo, R.; Talavera, E. M.; Alvarez-Pez, J. M. *Luminescence* **2002**, *17*, 233−235.

(10) Knutson, J. R.; Beechem, J. M.; Brand, L. *Chem. Phys. Lett.* **1983**, *102*, 501−507.

(11) Beechem, J. M.; Brand, L. *Photochem. Photobiol.* **1986**, *44*, 323−329.

(12) Janssens, L. D.; Boens, N.; Ameloot, M.; De Schryver, F. C. *J. Phys. Chem.* **1990**, *94*, 3564−3576.

(13) (a) Beechem, J. M.; Ameloot, M.; Brand, L. *Chem. Phys. Lett.* **1985**, *120*, 466−472. (b) Ameloot, M.; Beechem, J. M.; Brand, L. *Chem. Phys. Lett.* **1986**, *129*, 211−219. (c) Andriessen, R.; Boens, N.; Ameloot, M.; De Schryver, F. C. *J. Phys. Chem.* **1991**, *95*, 2047−2058. (d) Beechem, J. M.; Ameloot, M.; Brand, L. *Anal. Instrum. (N.Y.)* **1985**, *14*, 379−402. (e) Khalil, M. M. H.; Boens, N.; Van der Auweraer, M.; Ameloot, M.; Andriessen, R.; Hofkens, J.; De Schryver, F. C. *J. Phys. Chem.* **1991**, *95*, 9375−9381. (f) Van den Bergh, V.; Boens, N.; De Schryver, F. C.; Ameloot, M.; Gallay, J.; Kowalczyk, A. *Chem. Phys.* **1992**, *166*, 249−258.

(14) Ameloot, M.; Boens, N.; Andriessen, R.; Van den Bergh, V.; De Schryver, F. C. *J. Phys. Chem.* **1991**, *95*, 2041−2047.

(15) Anderson, D. H., Ed. *Lecture Notes in Biomathematics*; Springer-Verlag: Berlin, Germany, 1983.

(16) Meuwis, K.; Depuydt, G.; Boens, N.; De Schryver, F. C. *Chem. Phys. Lett.* **1995**, *246*, 641−648.

(17) Boens, N.; Basarić, N.; Novikov, E.; Crovetto, L.; Orte, A.; Talavera, E. M.; Alvarez-Pez, J. M. *J. Phys. Chem. A* **2004**, *108*, 8180−8189.

(18) Diehl, H.; Horchak-Morris, N. *Talanta* **1987**, *34*, 739−741.

(19) Johnson, M. L.; Frasier, S. G. *Methods Enzymol.* **1985**, *117*, 301−342.

(20) Maus, M.; Rousseau, E.; Cotlet, M.; Schweitzer, G.; Hofkens, J.; Van der Auweraer, M.; De Schryver, F. C. *Rev. Sci. Instrum.* **2001**, *72*, 36−40.

(21) Sjöback, R.; Nygren, J.; Kubista, M. *Spectrochim. Acta, Part A* **1995**, *51*, L7−L21.

(22) Klonis, N.; Sawyer, W. H. *J. Fluoresc.* **1996**, *6*, 147−158.

(23) Martin, M.; Lindqvist, L. *J. Lumin.* **1975**, *10*, 381−390.

(24) Leonhardt, H.; Gordon, L.; Livingston, R. *J. Phys. Chem.* **1971**, *75*, 245−249.

(25) Mchedlov-Petrossyan, N. O.; Mayorga, R. S. *J. Chem. Soc., Faraday Trans.* **1992**, *88*, 3025−3032.

(26) Isaacs, N. *Physical Organic Chemistry*, 2nd ed.; Longman Scientific & Technical: Essex, U.K., 1995.

(27) (a) Shah, J.; Joshi, N. B.; Pant, D. D. *Curr. Sci.* **1984**, *53*, 255−256. (b) Shah, J.; Pant, D. D. *Curr. Sci.* **1985**, *54*, 1040−1043.

(28) (a) Tolbert, L. M.; Haubrich, J. E. *J. Am. Chem. Soc.* **1990**, *112*, 8163−8165. (b) Tolbert, L. M.; Solntsev, K. M. *Acc. Chem. Res.* **2002**, *35*, 19−27.

(29) Boens, N.; Kowalczyk, A.; Cielen, E. *J. Phys. Chem.* **1996**, *100*, 4879−4887.

(30) Lide, D. R. *CRC Handbook of Chemistry and Physics*, 84th ed.; CRC Press: Boca Raton, FL, 2003.

(31) Rice, S. A. *Diffusion-Limited Reactions*; Comprehensive Chemical Kinetics, Vol. 25; Elsevier Biomedical: Amsterdam, 1985.